Landslides Triggered by the 2004 Niigata Ken Chuetsu, Japan, Earthquake

D. Scott Kieffer,[a)] M.EERI, Randy Jibson,[b)] M.EERI, Ellen M. Rathje,[c)] M.EERI, and Keith Kelson,[d)] M.EERI

The Niigata Ken Chuetsu earthquake triggered a vast number of landslides in the epicentral region. Landslide concentrations were among the highest ever measured after an earthquake, and most of the triggered landslides were relatively shallow failures parallel to the steep slope faces. The dense concentration of landslides can be attributed to steep local topography in relatively weak geologic units, adverse hydrologic conditions caused by significant antecedent rainfall, and very strong shaking. Many of the landslides could be discerned from high-resolution satellite imagery acquired immediately after the earthquake. [DOI: 10.1193/1.2173021]

INTRODUCTION

The Niigata Ken Chuetsu earthquake triggered a vast number of landslides that were densely concentrated in a mountainous area in central Niigata Prefecture. Landslides severely damaged roads and rail lines, destroyed houses and other structures, and dammed streams and rivers. Damage from the landslides has been initially estimated at U.S. $8 billion, making this one of the costliest landslide events in history. Several mountain villages have been rendered uninhabitable for the foreseeable future—and perhaps permanently, in some cases.

This paper summarizes the reconnaissance observations about the landslides, briefly describes the conditions in the area that contributed to slope instability, documents the number and concentration of landslides, describes observations of various landslide types and their resulting damage, and discusses how the landslides compare with those triggered by comparable earthquakes.

Several factors contributed to the extensive landsliding. Besides the steep local topography, the principal factors that contributed to slope instability include (1) the presence of weak, deformed geologic materials; (2) exceptionally high groundwater conditions both at depth and in surficial layers; and (3) very high levels of strong ground motion.

[a)] Colorado School of Mines, 1600 Illinois St., Golden, CO 80401
[b)] U.S. Geological Survey, 1711 Illinois St., Golden, CO 80401
[c)] University of Texas at Austin, 1 University Station C1792, Austin, TX 78712
[d)] William Lettis & Associates, 1777 Botelho Dr., Suite 262, Walnut Creek, CA 94596

Earthquake Spectra, Volume 22, No. S1, pages S47–S73, March 2006; © 2006, Earthquake Engineering Research Institute

LOCAL GEOLOGY

Bedrock in the area of the main landslide concentration consists of a folded sequence of Miocene to early Pleistocene sedimentary units consisting of weak and friable claystone and siltstone having fairly low durability, with interbedded sandstone and minor conglomerate. The sedimentary sequence represents a shallow marginal facies (Yanagisawa et al. 1986). The bedrock is blanketed locally by colluvium, and unconsolidated Pleistocene to Holocene alluvial deposits are present within river and stream channels and their floodplains. Young, weakly cemented materials such as this have produced high landslide concentrations in several well-documented earthquakes (e.g., Harp and Jibson 1995, 1996; Bommer and Rodríguez 2002; Jibson et al. 2004).

GROUNDWATER CONDITIONS

High antecedent rainfall was a major contributor to the large concentrations and densities of landslides. Japan sustained a record 10 typhoons in the months before the earthquake. In the days immediately before the earthquake, Typhoon Tokage struck, releasing large quantities of rainfall in the epicentral area: precipitation measured at Nagaoka was 100 mm on October 20 and 13 mm on October 21. Thus antecedent soil moisture conditions were highly unfavorable at the time of the earthquake. The exceptionally high seasonal rainfall, including a summer season of very high typhoon activity, probably resulted in regional groundwater conditions that contributed substantially to landsliding. Typhoon Tokage probably saturated surficial soils and thus contributed to shallow slope instability. For the argillaceous bedrock materials described above, these high antecedent moisture conditions would tend to cause softening and strength reduction as well as the undesirable effects of elevated pore or joint water pressures and seepage forces.

EARTHQUAKE SHAKING

The earthquake produced very high levels of ground motion in the epicentral area, including two sites that recorded peak horizontal ground accelerations of 1.3–1.8 g and several other sites that recorded accelerations greater than 0.3 g. A Japan Meteorological Agency (JMA) strong-motion station was in Yamakoshi, which is in the center of the landslide region. This station recorded peak horizontal ground accelerations of 0.55 g (NS) and 0.74 g (EW) and a peak vertical acceleration of 1.08 g. The earthquake occurred on a blind-thrust fault at a depth of 16 km. The area on the hanging-wall block directly above the fault rupture is steep terrain that produced most of the landslides.

OVERVIEW OF TRIGGERED LANDSLIDES

The landslides were primarily concentrated in the Uonuma hills east of Ojiya and north of Kawaguchi (Figure 1). The heaviest concentration of landsliding occurred near Yamakoshi on the hanging-wall block above the ruptured thrust fault. The EERI and GEER reconnaissance teams investigated much of the Yamakoshi region (Figure 1)—mostly on foot, since many roads had closed because of the landslides.

Most of the landslides were relatively shallow (1–2 m deep), slope-parallel failures of colluvial and residual soils mantling steep slopes. However, many deep failures also

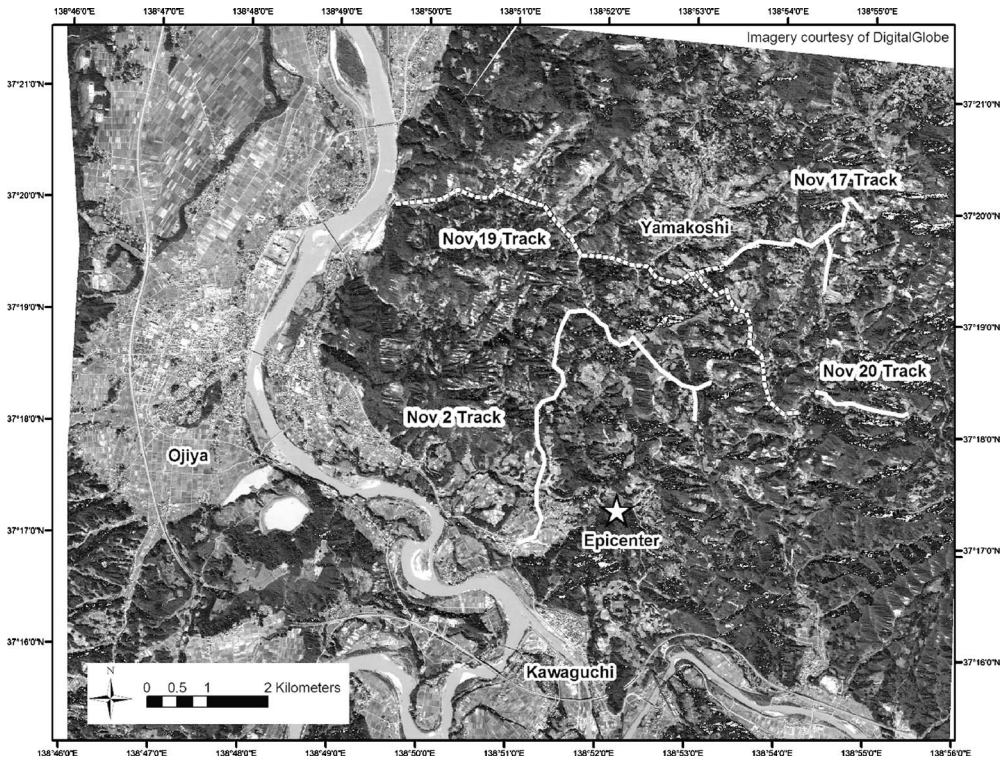

Figure 1. Satellite image of the landslide region, showing the routes—or "tracks"—of field reconnaissance (image: DigitalGlobe).

occurred, some of which had depths from several tens of meters to more than 100 m. Some of the landslides blocked streams and impounded small-to-large reservoirs. In some cases, landslides destroyed entire upland villages, causing major economic disruption.

In the zone of greatest landslide activity near Yamakoshi, landslide concentrations were estimated by using a landslide inventory map (at a scale of 1:30,000) that was based on aerial photos from October 25. This inventory, made by the Japan Geographical Survey Institute in 2004, primarily includes large landslides; thus it sampled only a subset of all the landslides. Even this partial inventory, however, shows very high landslide concentrations. In the 30-km^2 area of greatest landslide activity (Figure 2), concentrations as great as 30 landslides/km^2 were observed, and the average concentration of large landslides was 13.3 landslides/km^2. In comparison, worldwide data on earthquake-triggered landslides indicate maximum observed concentrations of about 13–14 landslides/km^2 at the epicenter, with concentrations decreasing markedly to about 1–2 landslides/km^2 at 5 km from the epicenter, and less than 1 landslides/km^2 at 10 km from the epicenter (Keefer 2002).

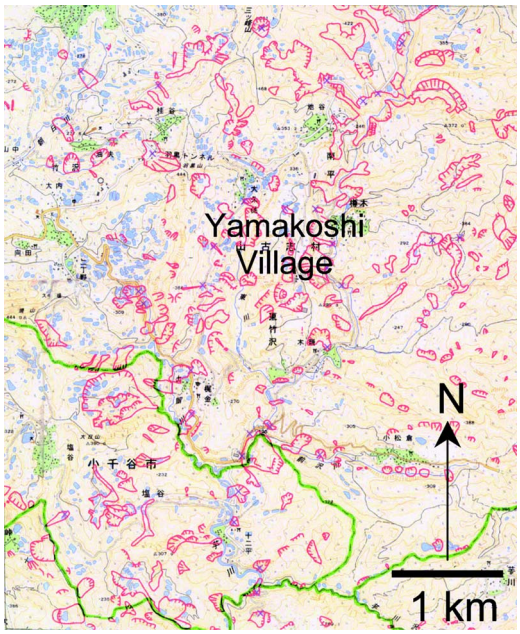

Figure 2. Landslide inventory map of an approximately 30-km^2 area in the epicentral region, based on aerial photos from 25 October 2004 (Japan Geographical Survey Institute).

The area covered by landslides (both source and deposit) is also quite large in comparison to worldwide earthquake data, although the quantitative worldwide data that can be used for comparison are limited. In the 30-km^2 study area were some 1-km^2 cells in which as much as 35% of the ground surface was covered by landslides. Over the entire 30-km^2 area, 17% of the ground surface (in map view) was covered by landslides. This is remarkably similar to landslide densities measured in the 1994 Northridge, California earthquake, which produced one of the highest landslide densities ever measured. Maximum landslide densities from the Northridge earthquake were about 35%, and densities over broader areas were as great as 17% (Parise and Jibson 2000). It must be emphasized that the estimated landslide concentrations and densities for the Niigata Ken Chuetsu earthquake were based on only a partial sampling of landslides (i.e., large landslides); if smaller slides were included in the inventory, then the concentrations and densities would be significantly larger than estimated in the present reconnaissance.

OBSERVATIONS OF LANDSLIDE TYPES AND EFFECTS

The reconnaissance teams visited numerous landslides in the epicentral region (Figure 1). Most of the triggered landslides were no more than a few meters deep and involved slope-parallel failures of colluvium, residuum, and highly weathered bedrock on steep slopes (>55°). Many shallow landslides mobilized into debris flows because of the high degree of soil saturation at the time of the earthquake, in some cases creating

Figure 3. Headscarp of a rotational failure along Highway 23 in the Yamakoshi epicentral area.

substantial landslide dams across alluvial floodplains. Had the earthquake struck during relatively dry conditions, probably fewer debris flows would have been triggered, and more landslides would have remained on the slope surfaces or moved only into the margins of the floodplains.

The limited scope of the reconnaissance mission prevented the teams from determining how many of the landslides were reactivated movements versus first-time movements. However, preliminary observations indicate that some pre-existing deep landslides were not remobilized during the earthquake. There was evidence that some of the landslides were being cleared away when the earthquake struck, suggesting that they had occurred in response to the heavy rainfall preceding the earthquake (Figure 3). Occurrence of pre-earthquake failure is evidenced by sandbags and caution fencing that are included within a larger, earthquake-induced failure of the road. Figure 4 shows another example of pre-earthquake slope instability along Highway 9. This section of the highway was impassable because of earthquake effects (Figure 5), so the sandbags at the base of the landslide must have been placed there before the earthquake.

There was also evidence that some failures had begun in response to aftershocks and/or rain that fell after the main shock. Figure 6 shows a fire truck parked across Highway 291 southeast of Yamakoshi City Hall, presumably to prevent vehicles from driving off a headscarp. Figure 7 shows the same fire truck in the distance and additional landslide damage in the foreground. The relatively intact section of road on which the fire truck is parked is only about 30 m long and has no fire station. This suggests that the truck was parked after a landslide that had been triggered during the main shock, but before a second landslide occurred that stranded the truck.

As described below, the landslide failure mechanisms comprise a broad spectrum, including shallow translational soil failures, deep rotational bedrock failures, large rock-

Figure 4. Slide debris deposited on sandbags that had been placed to stabilize a pre-existing rainfall-induced landslide along Highway 9 east of Nagaoka.

block slides, slump-flow complexes, and rapid debris flows. In some cases, deep bedrock landslides were clearly controlled by the rock-mass structure, and in other cases there was no apparent relation to structural discontinuities, and failure appeared to occur along curved shear surfaces more characteristic of soil slumping.

Figure 5. Damage to the roadway and to a retaining wall on Highway 9, east of Nagaoka.

Figure 6. Looking northwest, toward a fire truck that was parked across Highway 291 southeast of Yamakoshi City Hall to prevent vehicles from driving off a headscarp.

TRANSLATIONAL SOIL SLIDES

Slope-parallel failures involving colluvium, residuum, and highly weathered bedrock on steep slopes ($>55°$) represent most of the observed landslides. Although these failures were typically only a few meters deep, they covered extensive slope areas and produced great volumes of landslide debris that filled valley bottoms and locally blocked

Figure 7. Looking northwest on Highway 291, toward the same fire truck as in Figure 5. In the foreground is an additional roadway section destroyed by landsliding.

Figure 8. Shallow slope-parallel translational landslides along steep slopes near Yamakoshi.

floodplains (Figures 8 and 9). The failure surfaces commonly developed along the boundary with more intact and less weathered bedrock. Some slopes showed evidence of strong shaking that had stripped off most of the overlying soil mantle, leaving only a few fragments of partially mobilized soil mats (Figure 10). Typically, all vegetation was stripped off the surface, along with the soil cover.

Figure 9. North-facing valley wall, showing extensive translational soil sliding into the valley bottom in the Yamakoshi epicentral area.

Figure 10. Slope whose soil mantle was stripped off by strong shaking.

DEEP ROTATIONAL SLIDES

Deep rotational failures (slumps), with backward rotation resulting from shear along a curved failure surface, are typically associated with clay-rich soils. This failure mode is generally found only in rock masses that are relatively soft and free of weak seams or joints, or in rocks so highly fissured as to be effectively homogeneous. Rock types that can generate slumps are typically clay-rich rocks that have been softened by loosening and wetting, rock masses in and adjacent to major fault zones, and Tertiary sediments and coal-bearing rock formations (Goodman and Kieffer 2000). In most other rocks, the fracture of intact material tends to develop in response to tensile rather than shear stresses.

Heavy antecedent rainfall and a relatively young sedimentary sequence consisting mainly of weak and friable claystone and siltstone facilitated the development of rotational bedrock failures. In addition to the softening effect of high moisture conditions, the heavy and long-term seasonal rainfall probably significantly elevated pore pressures in the hillsides, exacerbating the potential for failure. Figure 11 shows an example of a deep rotational bedrock failure northeast of Shiotani (at the east end of the "Nov 2" track in Figure 1). Bedrock at this location consists primarily of Pliocene mudstone with interbedded sandstone of the Kawaguchi formation (Yanagisawa et al. 1986). The rotation of the slide is evidenced by a block of back-rotated trees and agricultural land bordering a headscarp to the left; the scarp is approximately 30 m high. Additional back-rotated blocks were present downslope, and the estimated maximum depth of the sliding surface is about 100 m.

ROCK-BLOCK SLIDES

Rock-block slides occurred in competent bedrock where adversely oriented discontinuities in the rock mass existed. Examples of block sliding along a single discontinuity surface were observed along the eastern side of the Shinano River near its confluence

Figure 11. Deep rotational bedrock slump northeast of Shiotani.

with the Asahi River, just west of Uragara (at the west end of the "Nov 19" track in Figure 1). Figure 12 shows two adjacent block slides approximately 300 m south of the confluence. These slides developed along a hogback composed primarily of Pliocene sandy mudstone of the Shiroiwa (White Rock) Formation (Yanagisawa et al. 1986); bedding dip slopes on the hogback are inclined at about 25°–30°. The ridge on which the slides occurred could represent the remnant of a much older and larger relict block slide from the higher ridges above.

Figure 12. Two adjacent rock-block slides south of Uragara, along Highway 291 (photo: Original Research Ideal Survey, http://www.oris.co.jp/jishin2004/h16jisin_k.htm).

Figure 13. Uragara rock-block slide formed by a bedding plane (sliding surface) and two sets of vertical joint release surfaces.

Figure 13 is a closer view of the block slide that appears at left in Figure 12. Sliding occurred along a dip-slope bedding plane and was facilitated by lateral releases provided by two sets of vertical joint surfaces. Figure 14 is a downslope view of the sliding plane and slide debris. The upright trees at the slide toe indicate pure translation of the debris over a distance of several tens of meters.

Figure 14. Downslope view of the Uragara slide plane and debris. The Shinano River is in the background.

Figure 15. Intact block of bedrock (to the left) contacting colluvial debris (to the right).

Exposed along the left lateral scarp of the block slide shown in Figures 13 and 14 is a geologic contact suggesting prior, perhaps ancient, slide movement. As shown in Figure 15, an intact block of bedrock has a steeply dipping and sharp contact with colluvial debris. This is interpreted as representing past block sliding of the material downslope of the contact, with subsequent infilling of the headscarp area with colluvial debris.

Immediately north of the confluence of the Shinano and Asahi rivers is the Shiroiwa landslide. This failure drew international attention because the landslide buried a mother and her two young children in their car. They were recovered about four days after the earthquake, and only one child survived. The ridge along which this failure occurred represents the northern extension of the hogback shown in Figure 12, and the bedrock again consists of Pliocene sandy mudstone of the Shiroiwa Formation (Yanagisawa et al. 1986). As shown in Figure 16, the block slide occurred at a re-entrant corner developed at the intersection of the eastern and southern sides of the Shinano and Asahi rivers, respectively. The compound slope configuration may have had two effects on the slide development: potential focusing of seismic energy and a reduction of kinematic constraint. For a structurally controlled slide to develop, whether a block slide or wedge slide, a minimum of four surfaces must be involved. The four surfaces are created by combinations of free surfaces as well as discontinuity surfaces. As Figure 16 shows, the hogback ridge and reentrant corner provide three free surfaces, so only one structural surface (a bedding plane) is required to liberate the mass. This is in contrast to the block slides shown in Figure 12, which necessitated structural release surfaces in addition to the bedding plane.

SLUMP-FLOW COMPLEXES

Slump-flow complexes within colluvium-filled swales and in areas of deep regolith and highly weathered bedrock represent another commonly observed mode of failure. The slump-flow complexes generally occurred on moderately steep slopes and typically

Figure 16. Looking northeast toward the Shiroiwa block slide at the confluence of the Shinano and Asahi rivers (photo: I. Yasuda, Hasshu Company).

had very long runout distances, probably because of the high antecedent moisture conditions. The slump-flow complex in Figure 17 ran out over multiple rice paddy terraces.

Figures 18 and 19 show a slump-flow complex along Highway 24 northeast of Ya-

Figure 17. Slump-flow complex in a colluvium-filled swale along Highway 9 east of Nagaoka (photo: I. Yasuda, Hasshu Company).

Figure 18. Northwest-facing slump-flow complex with a large headscarp at the top and debris in the foreground, on Highway 24 northeast of Yamakoshi City Hall.

makoshi City Hall. Figure 19 also shows the typical runout characteristics of slump-flow complexes triggered by the earthquake, which in this case destroyed several residential structures along its path.

DEBRIS FLOWS

The earthquake triggered many debris flows that had significant runout distances (Figure 20). In previous earthquakes worldwide, debris flows have occurred much less commonly than other types of landslides (Keefer 1984). However, owing to heavy antecedent rainfall, this earthquake triggered many large debris flows, some of which traveled long distances and were devastating.

LANDSLIDE DAMS

The earthquake triggered numerous landslide dams—at least dozens, and perhaps hundreds, of them—in the mountainous area around Yamakoshi. Most of the dams were relatively small blockages created by deposits of shallow landslides from steep-walled stream valleys (Figure 21). Typically, the impounded water extended only a few tens of meters upstream, but in some cases much larger reservoirs were created, some of which submerged roads and partially inundated small villages (Figure 22). At the time of the

Figure 19. Debris deposited by a northwest-flowing slump-flow complex, with destroyed buildings along the right margin, on Highway 24 northeast of Yamakoshi City Hall.

reconnaissance, most of the smaller blockages had already been overtopped, and relatively stable drainages had been reestablished so that sudden downstream inundation was unlikely. One notable exception is described below.

About 1 km west of Komatsugura (the west end of the "Nov 20" track in Figure 1), the earthquake triggered a large landslide that dammed the Imo River and impounded a reservoir that extended more than 1 km upstream as of November 20. The landslide

Figure 20. Large debris flow, exhibiting a narrow path and a long runout.

Figure 21. Damming of a tributary valley caused by rotational slides and roadway embankment failures in the Yamakoshi epicentral area.

(Figure 23) was a block slide along a dip slope composed of Pliocene sandy mudstone of the Shiroiwa formation (Yanagisawa et al. 1986), dipping about 20° west. A large graben formed at the head of the landslide as the slide mass moved across the canyon and completely blocked the drainage (Figure 24). At that date, the reservoir was rising about 15–20 cm/day, despite efforts to convey water over the dam in a controlled manner.

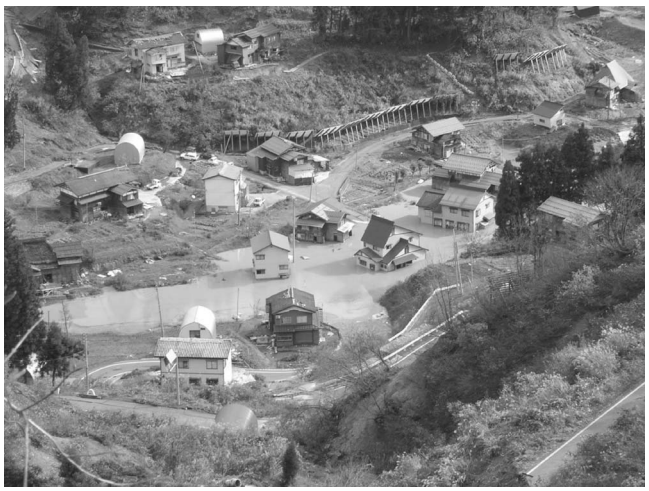

Figure 22. Looking east from Road 23 at the inundation of a tributary valley and houses upstream of a landslide dam in the Yamakoshi epicentral area.

Figure 23. Oblique aerial view of a landslide dam west of Komatsugura before the reservoir filled. The area in the center, which is enclosed by a line, shows the extent of the slide mass; small arrows show the uppermost extent of the main scarp; and the large arrow shows the movement vector. The bridge at left was completely submerged at the time of the reconnaissance, and the reservoir had backed up as far as the village shown in the upper left (photo: Kokusai Kogyo Company, Ltd.).

Figure 24. The upstream face of the Komatsugura landslide dam. The reservoir extends upstream to the right. The light gray area in the center left is a spillway being excavated and armored. Note several shallow landslides on the slopes in the background.

Figure 25. Landslide from a slope above a road east of Yamakoshi.

LANDSLIDE DAMAGE TO ROADS

Because of the high concentration of slope failures, the regional road network in the mountainous area around Yamakoshi was severely damaged. Although most observed landslides causing road damage are estimated to have volumes of a few hundred to a few thousand cubic meters, their collective volume is so significant as to pose a serious challenge for eventual reopening.

Observed landslide damage to the roadways occurred principally from three basic mechanisms: slope failure above roadways that had been excavated into steep hillsides (Figure 25), undermining of roadways because of slope failure below the roads (Figure 26), and failure of unsupported embankment fill (Figure 27).

Landslides damaged several retaining walls along roadways. Typically, the retaining walls were rather modest, presumably having been designed for active lateral earth pressures. Such walls cannot be expected to withstand forces induced by significant slope failure (Figure 28). Although slumps and slump-flow complexes were the most commonly observed types of landslides causing roadway damage, many damaging landslides were more complex. Figure 29 shows a slope failure involving back rotation (slumping) of the roadway. Close examination, however, shows that portions of the slide mass have rotated forward, indicating complex interaction between different blocks within the sliding mass.

OBSERVATIONS FROM SATELLITE IMAGERY

Several high-resolution commercial satellites have been launched since 2000 whose data have been used to document earthquake effects (e.g., Rathje et al. 2005). Post-earthquake satellite images of the affected region were acquired by the Quickbird satellite (www.digitalglobe.com) on October 24, only one day after the earthquake. This satellite collects data at resolutions as high as 0.6 m, which is sufficient for identifying

Figure 26. Source area of a slump-flow complex south of Yamakoshi.

terrestrial features such as buildings, roads, and landslides. The imagery was acquired with the satellite oriented at a 47° angle (as measured from the vertical). Ideal acquisition angles are 0°–15°, but a large acquisition angle was required in this case because of the satellite's orbit relative to Japan after the earthquake. The large acquisition angle distorts features in the image and creates some hidden areas behind hills and mountains. Nonetheless, the imagery provides useful information about the landslide distribution for this earthquake.

The Quickbird imagery was used to develop a rapid, preliminary estimate of the

Figure 27. Failure of a roadway embankment fill south of Yamakoshi.

Figure 28. Landslide damage to a retaining wall and adjacent roadway on Highway 291, southeast of Yamakoshi City Hall.

landslide distribution within the Yamakoshi region. Many of the earthquake-induced landslides are characterized by shallow sliding surfaces that stripped the overlying vegetation. Thus, the preliminary estimate of the landslide distribution was developed by identifying the nonvegetated areas in the mountainous Yamakoshi region. The landslide areas were identified by thematic classification of the 0.6-m-resolution pan-sharpened Quickbird imagery. This classification involved identifying the major thematic regions within the image (e.g., vegetation, landslides, urban areas, and water), defining training pixels for each thematic class, and performing a maximum likelihood classification of the image by using the spectral (color) information of each pixel. The maximum likelihood classification algorithm uses the training pixels to describe the statistics of the spectral data for each thematic class, then the algorithm uses this information to classify the remaining pixels in the image.

Figure 30 shows the landslides identified by the thematic classification of the satellite image. Most of the identified landslides are on the eastern slopes of the mountains, which is a result of the large acquisition angle from the east that hides many of the western slopes. There is a high density of landslides in the eastern and western sections of the image, which are generally coincident with the Pliocene sandstones and mudstones of the Shiroiwa and Kawaguchi formations. In the landslide classification, some light-colored areas are incorrectly identified as landslides in the flat farmlands north of Kawaguchi, because the spectral (color) characteristics in these areas are similar to those of the landslides.

Two areas of severe landsliding are delimited in Figure 30 and shown in detail in Figures 31 and 32. Figure 31 shows the area immediately east of the Shinano River, where the Shiroiwa landslide occurred and where the town of Uragara is located. Figure

Figure 29. Landslide damage to a roadway east of Yamakoshi. Note the backward rotation of the roadway and utility poles in the foreground, together with their forward rotation in the background.

31a shows a large landslide that is visible to the east of Uragara. This landslide is the apparent source of the mudslide material that flowed down a creek toward the Shinano River. In this figure, the road through Uragara is a light gray, indicative of fresh debris. The White Rock landslide is visible at the mouth of this creek, along the bank of the Shinano River, and apparently this landslide blocked at least part of the creek near the confluence. The block slides described earlier in Figures 12–15 are labeled in Figure 31a. In this photo, a large, light gray area south and west of these slides probably represents a mixture of water and debris that overflowed from a northeast-flowing incised creek that had been blocked by the landslides immediately east of the creek. Figure 31b shows the results of satellite-based landslide classification of this region. The black areas are identified as landslides and include both source areas and deposits.

Figure 32a displays the area of intense landsliding east of Yamakoshi. A significant portion of this image consists of light gray areas indicating vegetation that was stripped or covered by landslides. One of the major landslides in this area occurred at a dairy farm, which is labeled at the bottom left of the figure. Although some of the light gray

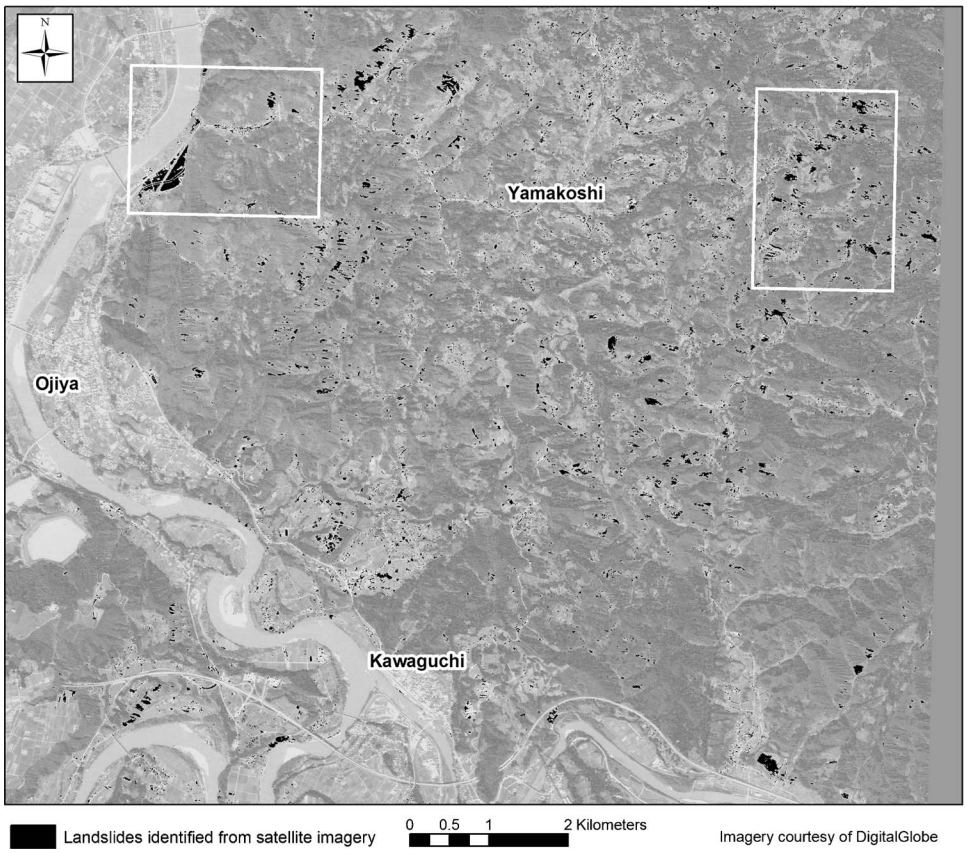

Figure 30. Landslides (which appear in black) in the epicentral region that were identified by using satellite imagery.

areas visible in this image correspond to rice fields, the interpretation of landslides in Figure 32b correctly identifies most of the landslides in the area, with only minimal confusion with rice fields.

DISCUSSION AND CONCLUSIONS

The Niigata Ken Chuetsu earthquake is analogous in many ways to the 1994 Northridge earthquake. Both nucleated on blind-thrust faults that did not produce surface fault rupture. The two earthquakes were of similar magnitude (Mw=6.7 for Northridge, and Mw=6.6 for Niigata Ken Chuetsu) and generated very high ground accelerations, particularly on the hanging wall above the thrust fault. (Harp and Jibson 1995, 1996). Moreover, geologic conditions were quite similar: both earthquakes occurred in areas of steeply sloping dissected terrain, within deformed and weakly cemented Pliocene and Pleistocene clastic sedimentary rocks. These similarities may explain some of the comparable patterns of landsliding in the two earthquakes.

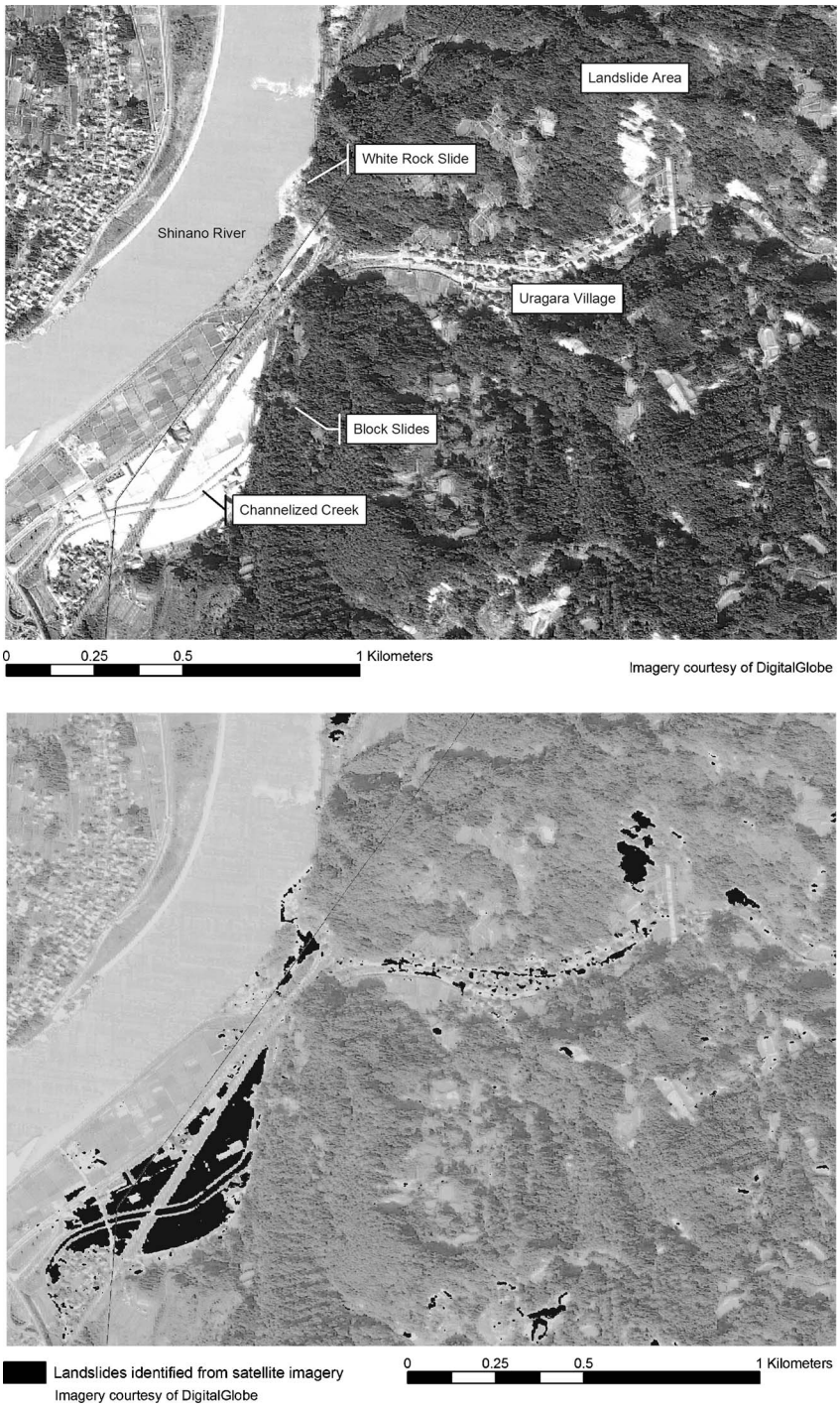

Figure 31. (a) Satellite image of the area around Uragara; (b) landslides (in black) identified by thematic classification of satellite imagery.

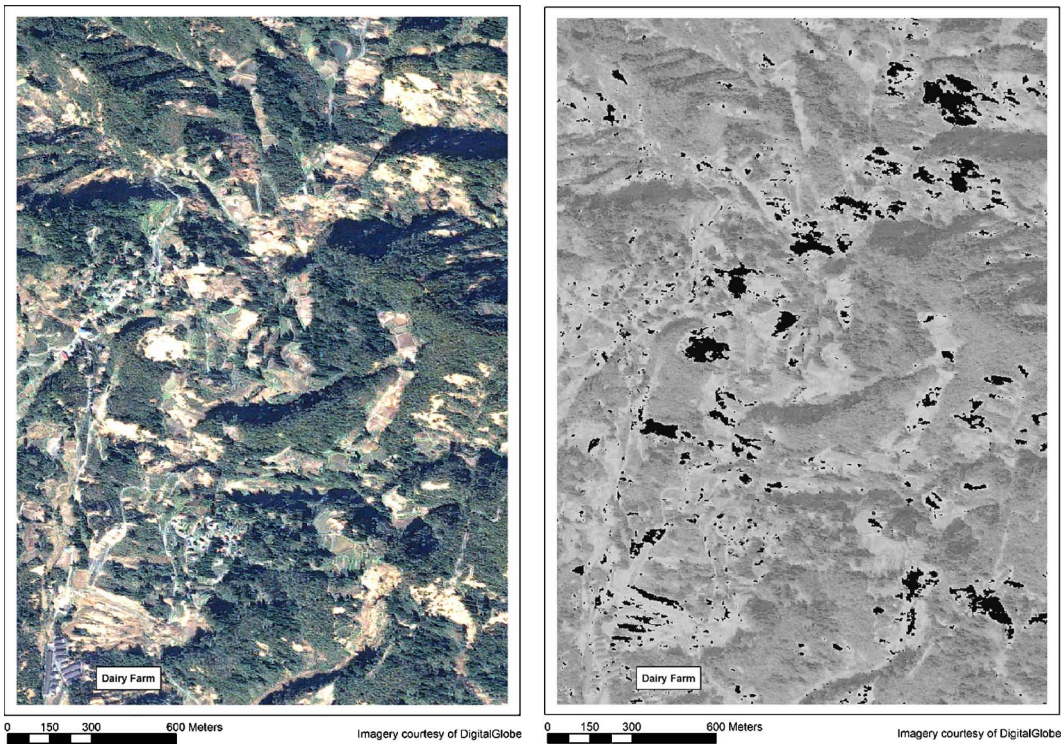

Figure 32. (a) Satellite image of an area east of Yamakoshi; (b) landslides (in black) identified by thematic classification of satellite imagery.

Both earthquakes triggered the greatest concentration of landslides in the steep terrain on the hanging wall above the thrust fault, and in both cases landslides were predominantly shallow, with disrupted landslides and falls in weathered rock and debris mantling the steep slopes. The area of greatest landslide concentration in the Niigata Ken Chuetsu earthquake, however, was much smaller, about 250 km^2, as compared with an area of about 1,000 km^2 of concentrated landsliding in the Northridge earthquake. Because the landslide-susceptible topography and geology appears to extend well beyond the zone of concentrated landsliding in the Niigata Ken Chuetsu earthquake, this difference could be attributable to differences in strong-motion attenuation.

A notable difference between these two earthquakes is the antecedent soil moisture conditions. The Northridge earthquake occurred when soils were completely dry, whereas the Niigata Ken Chuetsu earthquake struck when soils were probably saturated in many areas because of extremely heavy seasonal rainfall that continued until the earthquake. This probably explains the abnormally large number of debris flows triggered by the Niigata Ken Chuetsu earthquake. Generally, debris flows are fairly rare in earthquakes (Keefer 1984), but many highly saturated, mobile flows were triggered in the Niigata Ken Chuetsu earthquake. The large number of landslide dams may also have

resulted from the more saturated conditions: shallow failures from valley walls were more mobile and flowed into valley bottoms, creating blockages in streams that were flowing at fairly high levels. In the Northridge earthquake, many of the failures in dry material mobilized only partially and came to rest on slopes rather than moving all the way into valley bottoms (Harp and Jibson 1995, 1996).

The predominance of relatively shallow landslides observed after the Niigata Ken Chuetsu earthquake is consistent with observations from other earthquakes worldwide (Keefer 1984). Shallow failures indicate relatively high levels of high-frequency strong shaking (1–10 Hz). In past earthquakes, hanging walls above thrust faults have experienced abnormally high ground motions (Abrahamson and Somerville 1996, Dalguer et al. 2001) and consequent high concentrations of landslides (Harp and Jibson 1995, 1996; Jibson et al. 2004). Also, thrust earthquakes generally produce higher-frequency ground motion and higher accelerations than strike-slip events of similar magnitudes (Abrahamson and Silva 1997, Boore et al. 1997, Somerville et al. 1996). The very high ground accelerations reported for the Niigata Ken Chuetsu earthquake, with multiple stations recording accelerations significantly greater than 1 g (Mori and Somerville 2006, this issue), are consistent with this observation.

The dip slopes that produced the rock block slides have clearly experienced repeated episodes of sliding in the past. Interestingly, this earthquake triggered failure only within presumably undisturbed bedrock and not within the colluvium covering the slope (including some older failures). This suggests that the strength of the colluvial/bedrock contact exceeds the strength of whatever weak layer or discontinuity within the bedrock that has produced repeated episodes of block slides.

Although the landslide concentrations observed after this earthquake are quite high by worldwide historical standards (Keefer 2002), they still are much lower than in the Northridge earthquake, where concentrations greater than 100 landslides/km^2 were measured (Parise and Jibson 2000). This might seem odd, because the Niigata Ken Chuetsu earthquake occurred in much wetter conditions, which are generally associated with greater susceptibility to landslide generation. That discrepancy, however, is most likely attributable to the incomplete inventory of landslides from the Niigata Ken Chuetsu earthquake; the landslide inventory from the Northridge earthquake is much more comprehensive.

ACKNOWLEDGMENTS

Publication of this special issue on the Niigata Ken Chuetsu, Japan, earthquake was supported by the Learning from Earthquakes Program of the Earthquake Engineering Research Institute, with funding from the National Science Foundation under grant CMS-0131895. Any opinions, findings, conclusions, or recommendations expressed herein are the authors' and do not necessarily reflect the views of the National Science Foundation, the Earthquake Engineering Research Institute, or the authors' organizations.

REFERENCES

Abrahamson, N. A., and Somerville, P., 1996. Effects of the hanging wall and footwall on ground motions recorded during the Northridge earthquake, *Bull. Seismol. Soc. Am.* **86** (1B), S93–S99.

Abrahamson, N. A., and Silva, W. J., 1997. Empirical response spectral attenuation relations for shallow crustal earthquakes, *Seismol. Res. Lett.* **68**, 94–127.

Bommer, J. J., and Rodríguez, C. E., 2002. Earthquake-induced landslides in Central America, *Eng. Geol.* **63**, 189–220.

Boore, D. M., Joyner, W. B., and Fumal, T. E., 1997. Equations for estimating horizontal response spectra and peak acceleration from western North American earthquakes: A summary of recent work, *Seismol. Res. Lett.* **68**, 128–153.

Dalguer, L. A., Irikura, K., Riera, J. D., and Chiu, H. C., 2001. The importance of the dynamic source effects on strong ground motion during the Chi-Chi, Taiwan, earthquake: Brief interpretation of the damage distribution on buildings, *Bull. Seismol. Soc. Am.* **91**, 1112–1127.

Goodman, R. E., and Kieffer, D. S., 2000. Behavior of rock in slopes, *J. Geotech. Geoenviron. Eng.* **126**, (8) 675–684.

Harp, E. L., and Jibson, R. W., 1995. Inventory of Landslides Triggered by the 1994 Northridge, California Earthquake, *Open-File Rep./U.S. Geol. Surv. 95–213*.

Harp, E. L., and Jibson, R. W., 1996. Landslides triggered by the 1994 Northridge, California, earthquake, *Bull. Seismol. Soc. Am.* **86** (1B), S319–S332.

Jibson, R. W., Crone, A. J., Harp, E. L., Baum, R. L., Major, J. J., Pullinger, C. R., Escobar, C. D., Martínez, M., and Smith, M. E., 2004. Landslides triggered by the 13 January and 13 February 2001 earthquakes in El Salvador, in *Natural Hazards in El Salvador: Geological Survey of America Special Paper 375*, edited by W. I. Rose, J. J. Bommer, D. L. López, M. J. Carr, and J. J. Major, pp. 69–88.

Jibson, R. W., Harp, E. L., Schulz, W., and Keefer, D. K., 2004. Landslides triggered by the 2002 Denali Fault, Alaska, earthquake and the inferred nature of the strong shaking, *Earthquake Spectra* **20**, 669–691.

Keefer, D. K., 1984. Landslides caused by earthquakes, *Geol. Soc. Am. Bull.* **95**, 406–421.

Keefer, D. K., 2002. Investigating landslides caused by earthquakes—A historical review, *Surv. Geophys.* **23**, 473–510.

Mori, J., and Somerville, P., 2006. Seismology and strong ground motions in the 2004 Niigata Ken Chuetsu, Japan, earthquake, 2004 Niigata Ken Chuetsu, Japan, Earthquake Reconnaissance Report, edited by C. Scawthorn and E. Rathje, *Earthquake Spectra* **22** (S1) January (this issue), S1–S8.

Parise, M., and Jibson, R. W., 2000. A seismic landslide susceptibility rating of geologic units based on analysis of characteristics of landslides triggered by the 17 January, 1994 Northridge, California earthquake, *Eng. Geol.* **58**, 251–270.

Rathje, E. M., Woo, K., Crawford, M., and Neuenschwander, A., 2005. Earthquake damage identification using multitemporal high-resolution optical satellite imagery, International Geoscience and Remote Sensing Symposium, IEEE, Seoul, South Korea, July.

Somerville, P., Saikia, C., Wald, D., and Graves, R., 1996. Implications of the Northridge earthquake for strong ground motions from thrust faults, *Bull. Seismol. Soc. Am.* **86** (1B), S115–S125.

Varnes, D. J., 1978. Slope movement types and processes, in *Landslides Analysis and Control*, edited by R. L. Schuster, and R. J. Krizek, R. J., Transportation Research Board, National Academy of Science, Special Report 176, pp. 11–33.

Yanagisawa, Y., Kobayashi, I., Takeuchi, K., Tateishi, M., Chihara, K., and Kato, H., 1986. Geology of Ojiya District, Geological Survey of Japan, Quadrangle Series, Niigata (7), no. 50, scale 1:50,000 (in Japanese, with English abstract).

(Received 9 July 2005; accepted 9 December 2006)